J Mater Sci (2017) 52:9546–9557

Composites

A self-assembly of graphene oxide@Fe_3O_4/metallo-phthalocyanine nanohybrid materials: synthesis, characterization, dielectric and thermal properties

Antonio Eufrazio da Costa Júnior[1,*], João Paulo Ferreira Mota[1], Sheyliane Maria Adriano Pontes[1], Francisco Jonas Nogueira Maia[1], Claudenilson da Silva Clemente[1], Pierre Basílio Almeida Fechine[2], Felipe Bohn[3], Antonio Jefferson Mangueira Sales[4], Antônio Sérgio Bezerra Sombra[4], Luigi Carbone[5], Giuseppe Mele[6], Diego Lomonaco[1], and Selma Elaine Mazzetto[1]

[1] *Laboratório de Produtos e TecnologiaemProcessos (LPT) - Departamento de Química Orgânica e Inorgânica, Universidade Federal do Ceará, 6021, Fortaleza, CE 60440-900, Brazil*

[2] *Grupo de Química de Materiais Avançados (GQMAT) - Departamento de Química Analítica e Físico-Química, Universidade Federal do Ceará, Campus do Pici, Fortaleza, Brazil*

[3] *Departamento de Física, Universidade Federal do Rio Grande do Norte, Natal 59078-900, Brazil*

[4] *Laboratorio de Telecomunicações e Ciência e Engenharia de Materiais (LOCEM), Departamento de Física, Universidade Federal do Ceará UFC, Campus do Pici, Fortaleza, Brazil*

[5] *CNR NANOTEC-Istituto di Nanotecnologia c/o Campus Ecotekne Università del Salento, Via Monteroni, 73100 Lecce, Italy*

[6] *Dipartimento di Ingegneria dell'Innovazione, Università del Salento, Via Arnesano, 73100 Lecce, Italy*

Received: 20 January 2017
Accepted: 22 April 2017
Published online: 1 May 2017

ABSTRACT

In this work, we report the synthesis of novel inorganic–organic hybrid nanomaterials (GO@Fe_3O_4/CuPc) and GO@Fe_3O_4/ZnPc) consisting of sheets of graphene oxide (GO) decorated by iron oxide nanoparticles (Fe_3O_4), the whole heterostructure functionalized with metallo-phthalocyanines (MPc, M ≡ Cu or Zn). First the synthesis of nanomaterial (GO@Fe_3O_4) was prepared by hydrothermal self-assembly process through the mixture of graphene oxide and Fe^{+2}/Fe^{+3} salt solution. The metallo-phthalocyanines anchorage on the surface of nanosystem was lately performed by facile and effective ultrasonication method. The structure, composition and morphology of nanohybrids and intermediates were investigated by Fourier transform infrared spectroscopy, X-ray diffraction, thermogravimetric analysis, differential scanning calorimetry, UV–visible spectroscopy, scanning and transmission electron microscopy and impedance spectroscopy. All the results suggested that iron-based nanoparticles were successfully deposited onto graphene oxide sheet networks in the form of Fe_3O_4, forming nanospheres, decreasing in lattice defects of the GO sheets and dramatically increasing the dielectric properties of nanosystems. Nanomaterials presented saturation magnetization in the 52–58 emu/g and superparamagnetic

Address correspondence to E-mail: eufraziojr@yahoo.com.br

DOI 10.1007/s10853-017-1133-3

behavior. It was observed that the values of dielectric constant decreased as a function of the amount of phthalocyanines in the nanomaterials. Therefore, because of their versatile magnetic and dielectric performances, the novel superparamagnetic hybrid nanomaterials, herein described, can be considered as potential for microwave devices.

Introduction

According to the recent studies, nanoparticles (NPs) including magnetite (Fe_3O_4) and maghemite (Fe_2O_3) have attracted the attention of many researchers because of their unique physical and chemical properties [1, 2]. Their exclusive properties physical, magnetic and optical are attributed to nanoscale phenomena [3]. In particular, the magnetite has been widely investigated and proved to be useful for the development of novel nanomaterials and biomaterials with great potential the application for various areas as biomedical, nanoscience and biotechnology. Besides the traditional application, recently some deserve greater emphasis, cancer therapy [4], catalysis [5], biosensors [6], controlled drug delivery [7] and magnetic resonance imaging [8]. However, despite the large number of application of magnetic nanoparticles, recent studies show that the combination with other compounds has generated nanostructured hybrids with distinct properties and high performance [9]. These monohybrid materials have attracted special attention the past years as a result of opening novel perspectives in other areas of research involving the nanoscience and nanotechology due to the possibility of achieving enhanced properties or specific advanced functional materials [10]. Nanohybrid materials are formed from the combination of at least two components that interact on a molecular level, such as surfactant–nanoparticles metal [10], nanoparticles iron–biopolymers [11] and nanoparticles–macromolecules [12]. Study reported in the literature has been shown that magnetic nanohybrid materials can be of great use to absorb microwave, owing to their advantages over pure magnetite with respect to low cost, low dielectric loss, design flexibility and dielectric properties [13–15]. Antunes et al. [12] have synthesized phthalocyanine–Fe_3O_4 hybrid materials, and the results showed that as-prepared hybrid exhibited excellent magneto-optical property. Recently, the graphene oxide@Fe_3O_4–cellulose nanohybrid materials were prepared via solvothermal method by introducing the Fe_3O_4 nanoparticles in the graphene oxide sheets [16].

Graphene oxide (GO), a promising carbon-based material, shows excellent mechanical properties, large surface area and distinctive two-dimensional (2D) structure; furthermore, it contains versatile oxygen functional groups (hydroxyl, epoxide and carbonyl groups) located on the basal planes and edges of the 2D lattice, providing an ideal platform to anchor functional groups or moieties as nanoparticles and/or macromolecules. Their wide uses include research areas such as microelectronics [17], sensing [18], photocatalysis [19], biomedicine [20], dye-sensitized solar cells [21], drug delivery [22], electromechanical [23] and supercapacitors [24]. The presence of oxygenated functional groups confers to GO a significant polarity, thus making it compatible with materials that have similar dipolar character, as well as contributes to effectively improve the interfacial interactions between the free hydroxyls and the surface of magnetic nanoparticles. Thus, functional groups on the GO surface provide abundant reaction sites useful in the functionalization chemical. Recent studies have proved how organometallic compounds, showing a π-electron-conjugated system as, for instance, metallo-phthalocyanine, can be adsorbed/intercalated onto/into GO or other examples of layered carbon materials [25]. Yang et al. reported the synthesis of cobalt phthalocyanine–graphene oxide (CoPc–GO) nanostructures. The functionalizing driven force could be attributed to the strong π–π interaction between the molecules of the phthalocyanine and oxygenated groups present on the graphene oxide surface [26].

Copper phthalocyanine (CuPc) and zinc phthalocyanine (ZnPc) represent a class of molecules presenting a π-electron system highly conjugated, with unique chemical properties and wide applications in sensors [27], photocatalysts [28], electrocatalysts [29], supercapacitors [30], solar cell [31], transistors [32],

semiconductors [33], optical data storage devices [34], photodynamic therapy agents [35], liquid crystals [36], nonlinear optics [37] and organic electronics and optoelectronics [38]. Among such applications, the dielectric performances represent a key parameter to be investigated for electronic aims.

The synthesized phthalocyanines give greater solubility to the nanosystem in organic solvents. Unsubstituted phthalocyanines show poor solubility in organic solvents. However, the literature reports that phthalocyanines substituted with compounds with extensive alkyl chain increase solubility in organic solvents [35]. Thus, the use of Pc substituted with cardanol (which has an alkyl chain of up to 15 carbons) widens its range of use in several solvents. In addition, our study showed that the presence of Pc in the nanosystem did not significantly interfere in the dielectric and magnetic properties. This allows its application in dielectric–magnetic devices. A further advantage is that the thermal properties of the nanohybrid are improved with the incorporation of the Pc.

In the present paper, we report a facile and effective approach of preparation of GO@Fe_3O_4/MPc nanostructured hybrid materials using GO sheets as nanoscale building blocks, surface-doped with Fe_3O_4 nanoparticles and metallo-phthalocyanine, the latter synthesized from cardanol, a compound derived from cashew nut shell liquid (CNSL), which is a biomass-derived renewable sources. The main purpose of the paper is to investigate possible interactions between Fe_3O_4 nanoparticles, GO and phthalocyanine at the supramolecular level. For this aim, we used several techniques to characterize the final samples including scanning electron microscopy (SEM), Fourier transform infrared spectroscopy (FTIR), X-ray diffraction (XRD), thermogravimetric analysis (TGA) and differential scanning calorimetry (DSC). In addition, dielectric properties, spectroscopic and thermal stability of the GO@Fe_3O_4/MPc nanohybrids are also investigated in detail.

Experimental

The reagents used in this work were from Sigma-Aldrich, Vetec, Dynamics, Synth and Acros Organic and were used without prior purification. Solvents were previously distilled before their use. GO was prepared by a modified Hummer's procedure [39, 40]. Tetrakis-(3-pentadecylphenoxy)phthalocyanine metallated with copper and zinc were synthesized in our laboratory, according to the method reported in Ref. [41].

Preparation of GO@Fe_3O_4

Typical synthesis of GO@Fe_3O_4 nanohybrid material was carried out in a hydrothermal system by promoting the nucleation of iron oxide nanoparticles onto GO sheets. Briefly, 0.5 g of GO was first dispersed in 400 mL of water under ultrasonication for 60 min, whereas 0.1428 g of $FeCl_3{\cdot}6H_2O$ and 0.0525 g of $FeCl_2{\cdot}4H_2O$ (2:1 molar ratio) were dissolved in 20 mL of water. The Fe^{3+}/Fe^{2+} stock solution was added dropwise to the GO solution during constant stirring; then, the pH of the solution was adjusted to 9–10 by 30% ammonia solution. The as-obtained Fe_3O_4@GO black solid was washed with methanol (3 × 20 mL) and separated with the aid of neodymium magnet, dried at 60 °C and stored under vacuum conditions.

Preparation of GO@Fe_3O_4/CuPc and GO@Fe_3O_4/ZnPc

GO@Fe_3O_4/CuPc inorganic–organic hybrid material nanospheres were prepared by following the procedure hereafter detailed. 0.020 g of GO@Fe_3O_4 was dissolved in 2 mL of water under ultrasonication for 30 min. Afterward, a chloroform solution (1 mL) containing 0.050 g of CuPc was added to the inorganic systems and sonicated for 2 h at 45 °C. The dark brown product was washed several times with ethanol and stored under vacuum conditions. The same procedure was used in the case of ZnPc to produce Fe_3O_4@GO/ZnPc nanostructured hybrids.

Characterization

FTIR spectra were recorded in the range 4000–400 cm^{-1} with a Perkin-Elmer Spectrum One spectrophotometer, and samples were prepared using KBr pellets. Absorption spectra were recorded with a Varian Cary 5000 spectrophotometer. TGA was conducted under N_2 atmosphere (50 mL/min) using a Mettler–Toledo TGA/SDTA851e and analyzed at a heating rate of 10 °C/min. Samples of

10 mg were heated from 25 to 800 °C. DSC analysis was carried out under N_2 atmosphere (50 mL/min) at a heating rate of 10 °C/min using Mettler–Toledo DSC823e heated from 25 to 400 °C, in platinum crucible; sample mass used in this experiment was 5 mg. SEM analyses were performed with a Quanta FEG 450 equipped with EDS/EBSD at 10–20 kV, and the samples overcoated with 10 nm of gold (Q 150t ES, Quorum). The samples' morphologies were analyzed with Jeol JEM-1011 TEM operating at 100 kV and equipped with a CCD camera ORIUS 831. The XRD analysis was performed in an X-ray powder diffractometer Xpert Pro MPD (Panalytical) using Bragg–Brentano geometry in the range of 5°–80° with a rate of 1° min^{-1}. CoKα radiation ($\lambda = 1.7889$ Å) was used, and the tube operated at 40 kV and 30 mA. The dielectric measurements were obtained in an impedance analyzer Solatron model SI 1260 equipped with an accessory (Sample Holder-1296A), to investigate dielectric behavior at room temperature (25 °C). The real (ε') part and imaginary (ε'') part of relative permittivity and dielectric loss factor ($\tan \delta = \varepsilon''/\varepsilon'$) were thus measured.

Results and discussion

The coexistence in the nanohybrid synthesis product of GO, magnetic Fe_3O_4 nanoparticles and MPc molecules was originally detected by FTIR (Fig. 1), one critical characterization technique which allows a quick and efficient identification of molecular chemical groups and their interaction thereof [24]. In all the spectra, a very broad intense peak at ~3425 cm^{-1}, due to O–H stretching vibration, was distinct. Concerning the pure GO sample, peaks at 1730 and 1630 cm^{-1} were attributed to C=O and –OH bands, respectively (Fig. 1a). Then, the peak at 1390 cm^{-1} was assigned to the bending vibration of O–H, whereas the peaks at 1221 and 1022 cm^{-1} were attributed to the C–O–C epoxy and C–O alkoxy groups stretching vibrations [39]. Figure 1b displays the FTIR of GO@Fe_3O_4 nanoachitecture. A strong absorption band at ~560–580 cm^{-1}, attributed to stretching vibration of Fe–O in tetrahedral site [42, 43], evidenced the presence of the magnetite nanoparticles on the GO interlayer spacing. Similarly, two peaks at 3410 and 1633 cm^{-1} were attributed to the presence of hydroxyl groups that reside at the Fe_3O_4 nanoparticles surface and uniquely due to O–H stretching and angular vibration, respectively. Figure 1b also presents bands at 3410, 1630, 1390, 1221 cm^{-1}, vibrations characteristic of the functional chemical groups present in the GO, as previously mentioned. Further, disappearance of the signal at 1728 cm^{-1} in the GO@Fe_3O_4 spectrum with respect to pure GO suggests possible interaction of graphite oxide –COOH groups with the free hydroxyls of the magnetite by hydrogen bonds. The functionalization of GO@Fe_3O_4 with CuPc (Fig. 1c) was confirmed by the presence of characteristics absorption bands typical of C–H of aliphatic chains (2918 and 2848 cm^{-1}) of cardanol and absorption bands at 1610, 1582, 1470 and 1445 cm^{-1}, attributable to the stretching vibrations of the bond C–C of the aromatic rings. Similar features are presented in Fig. 1d, showing the FTIR analysis of GO@Fe_3O_4/ZnPc nanohybrid material.

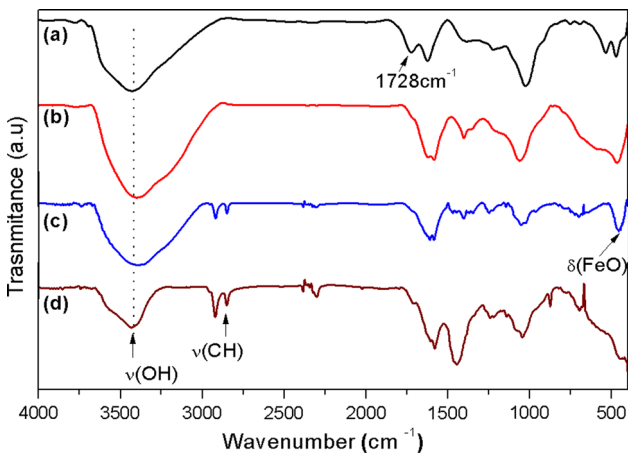

Figure 1 FTIR spectra of (*a*) GO, (*b*) GO@Fe_3O_4, (*c*) GO@Fe_3O_4/CuPc and (*d*) GO@Fe_3O_4/ZnPc, respectively.

The effectiveness of functionalization with metallophthalocyanine could be further confirmed by UV–Vis analysis (Fig. 2). The bands at 352 and 680 nm are characteristic absorption bands of ZnPc [44]. Furthermore, compared with the spectrum of GO, a shoulder peak shift from 250 to 280 nm can be observed. Such red shift is attributed to the strong π–π interaction between GO and grafted ZnPc in GO@Fe_3O_4/ZnPc, leading to the relocation of the electrons from graphene sheets to the zinc phthalocyanine group in the heterostructure [44]. The same behavior was observed for Cu phthalocyanine-based hybrid nanoarchitecture. In fact, a more significant alteration of the intensity profile of the absorption band in the case of GO@Fe_3O_4/CuPc nanohybrid could be noticed. For instance, the peak that in the

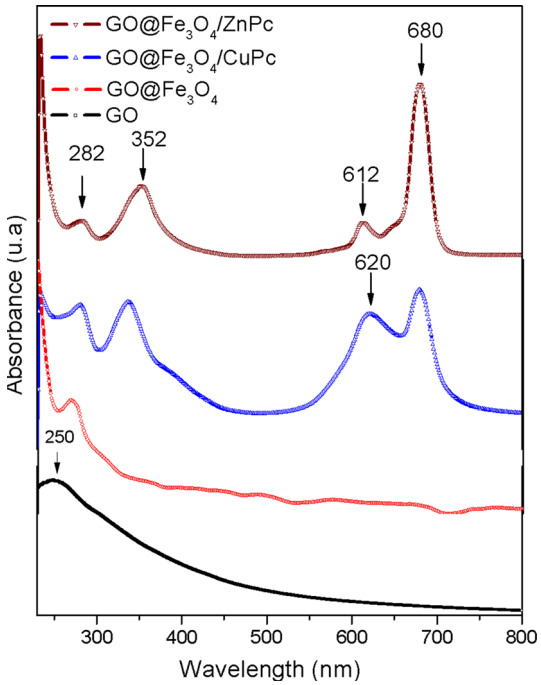

Figure 2 UV–Vis spectra of GO, GO@Fe_3O_4, GO@Fe_3O_4/CuPc and GO@Fe_3O_4/ZnPc.

case of ZnPc was located at 612 nm showed an intensity increase and a redshift to 620 nm in the case of CuPc, reasonably caused by a strongest adsorption and/or intercalation onto carbon sheets.

Figure 3 shows the TGA curves of GO, GO@Fe_3O_4, GO@Fe_3O_4/CuPc and GO@Fe_3O_4/ZnPc nanohybrids. The thermogravimetric curve of GO showed three main stages of weight losses, respectively, at

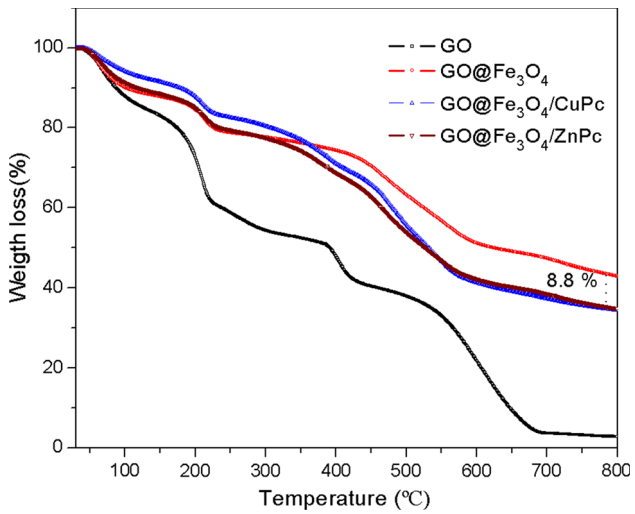

Figure 3 TGA curves of GO, GO@Fe_3O_4, GO@Fe_3O_4/CuPc and GO@Fe_3O_4/ZnPc.

150 °C (18 wt%), 220 °C (22 wt%) and 380 °C (10 wt%). In agreement with previous reports in the literature, the firsts loss has been attributed to evaporation of adsorbed water, and the others, respectively, to decomposition of labile oxygen deriving from functional groups such as hydroxyl, epoxy and carbonyl [45] and to the removal of more stable oxygen functionalities deriving from phenol, carbonyl and quinone [44, 46]. The thermogram of GO@Fe_3O_4 shows a 22% of weight loss at 250 °C, then a further 4% of loss in the range of 250–400 °C and 24% above 400 °C (400–600 °C). The final residual weight at 800 °C was roughly of 43%. The high residual weight of GO@Fe_3O_4 is interpreted in light of the presence of Fe_3O_4 nanoparticles adsorbed in the layers among GO sheets. The TGA curves of GO@Fe_3O_4/CuPc and GO@Fe_3O_4/ZnPc nanohybrids showed profiles similar to GO@Fe_3O_4, although they revealed a difference of weight loss of 8.8% in relation to GO@Fe_3O_4 system, in the temperature range 350–800 °C. This is attributed to the thermal decomposition of metallophthalocyanine covalently attached to graphene oxide sheets. The DSC scans for the GO, GO@Fe_3O_4 and MPc-functionalized magnetic nanohybrids are shown in Fig. 4. One can observe that all the samples have two characteristic events observed in the endothermic and exothermic transition which can be associated with dehydration and decomposition of respective nanomaterials. The thermograms of the GO (1) and the GO@Fe_3O_4 (2) presented two thermal stages: the first endothermic (peak 64 °C and enthalpy 437.08 J g^{-1}) was attributed to water adsorption between the sheets of the GO, whereas the second exothermic event (peak centered at 217 °C and enthalpy 723.66 J g^{-1}) could be attributed to the decomposition of labile oxygen functional groups, yielding CO, CO_2 of the GO [45, 47]. Both are in the accordance with TGA data wherein a mass loss below 150 °C was observed, as due to water evaporation, whereas the second feature could be ascribed to the decomposition of the oxygenated chemical functions that are part of the structure of the GO. Table 1 summarizes all the information with thermal parameters including the enthalpy obtained from the integration of the DSC curves of the thermal events, temperature range and peak position of the events. The anchoring of the phthalocyanines on the GO surface was confirmed by the appearance of a small endothermic feature below 50 °C, with enthalpy between 10 and 19 J g^{-1}, which was attributed to

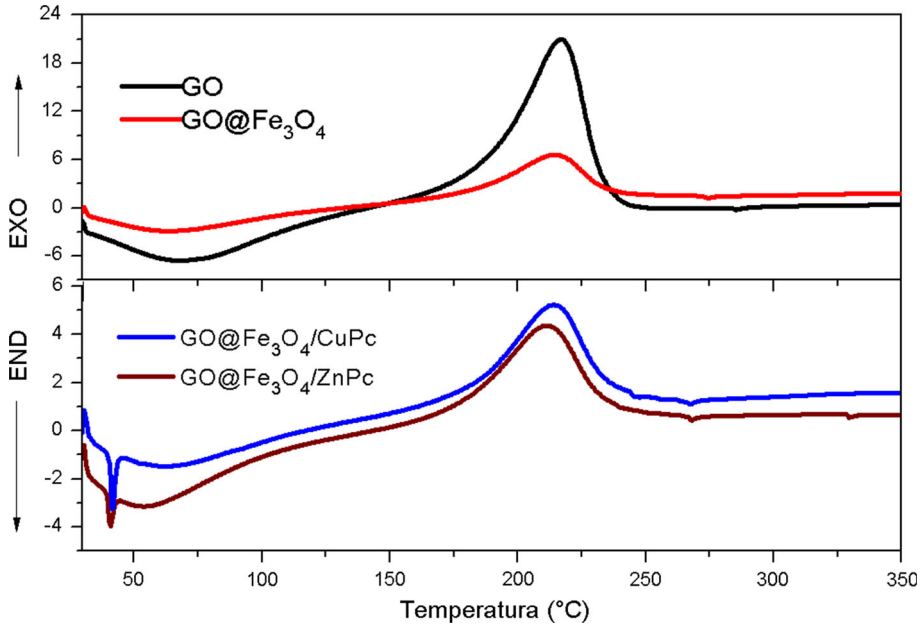

Figure 4 DSC curves of GO, GO@Fe_3O_4, GO@Fe_3O_4/CuPc and GO@Fe_3O_4/ZnPc.

Table 1 Thermal parameters: enthalpy, thermal events, temperature range and peak of the events obtained from of the DSC curves

Samples	Events thermal					
	Endothermic event			Exothermic event		
	Temperature range (°C)	Peak(°C)	Enthalpy (J g^{-1})	Temperature range (°C)	Peak(°C)	Enthalpy (J g^{-1})
GO	30–150	68	–437.08	150–250	217	723.66
GO@Fe_3O_4	30–150	64	–163.76	150–250	214	307.50
GO@Fe_3O_4/Cu(Pc)	38–45	41	–19.06	150–250	212	192.32
GO@Fe_3O_4/Zn(Pc)	38–45	37	–10.13	150–250	212	257.55

phase transition presented by phthalocyanine in this temperature range [48]. Thus, based on the results by FTIR, TGA and DSC, we can affirm that the phthalocyanines were incorporated in the nanoarchitectures, reasonably interacting with the surfaces of the graphene sheets.

The magnetic hysteresis curves of nanohybrids were performed at room temperature by using a vibrating sample magnetometer as shown in Fig. 5. The magnetization curves of all samples exhibit a strong magnetic response to magnetic field variation and a characteristic superparamagnetic behavior. The values of saturation magnetization (Ms) found for Fe_3O_4, GO@ Fe_3O_4, GO@ Fe_3O_4/CuPc and GO@ Fe_3O_4/ZnPc were 58.60, 54.65, 53.48 and 52.03 emu g^{-1}, respectively. In general, the magnetization values obtained from the hybrid materials are slightly smaller than those of the pure magnetite (60 emu g^{-1}), in totally agreement with similar examples reported in the literature [49]. At first sight, such discrepancies in the magnetization values are reasonably due to the various contents of GO sheets existing in the hybrid materials and of metallo-phthalocyanines adhering onto their surfaces. Nevertheless, it is also to be noted that graphene oxides and metallo-phthalocyanines are materials with no hysteresis curve; therefore, when they adhere to the surface of magnetite, they act as insulators, reducing the action of the magnetic field and consequently disfavoring the alignment of the spins contained in the magnetite domains. This effect promotes the reduction in the saturation values of the magnetization presented by this nanomaterial. The nanohybrids, dispersed into ethanol, can be rapidly separated (within 20 s) by a small neodymium magnet, as shown in Fig. 5.

The GO@Fe_3O_4 nanohybrid crystalline structure and size were initially investigated by XRD analysis

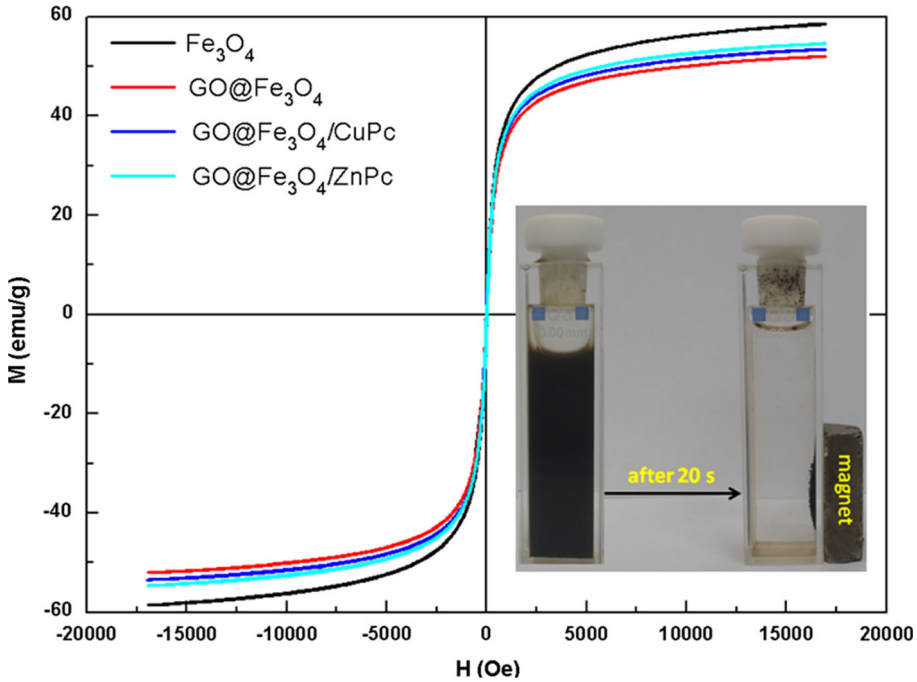

Figure 5 Magnetization curves of the samples: GO, GO@Fe_3O_4, GO@Fe_3O_4/CuPc and GO@Fe_3O_4/ZnPc.

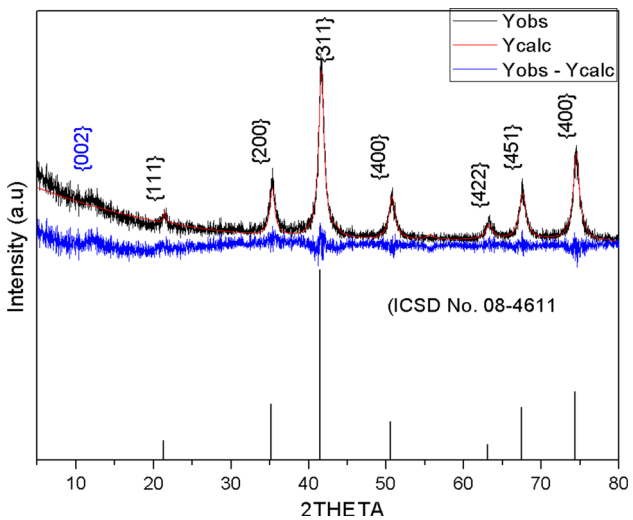

Figure 6 XRD analysis of GO@Fe_3O_4 heterostructures.

(Fig. 6). The blue lines represent the relative difference between the experimental (YExp) and calculated (YCalc) intensities obtained by the Rietveld refinement. The diffraction patterns showed that the main reflection peaks at $2\theta = 21.37°$ {111}, 35.16° {220}, 41.45° {311}, 50.56° {400}, 63.09° {422}, 67.37° {511}, 74.44° {440} can be well indexed with the reference pattern of the Fe_3O_4 inverse cubic spinel structure (ICSD/PDF 08-4611). The powder XRD pattern of GO@Fe_3O_4 showed a relatively low peak at $2\theta = 11.60°$ ($d = 8.6$ Å), corresponding to the diffraction in {002} graphene oxide plane. The full width at half maximum (FWHM) corresponding to {311} peak from XRD patterns along with the calculated crystallize size by Scherrer's equation showed a magnetite nanoparticles average size of about 12 ± 2 nm and microstrain obtained by Williamsom–Hall equation [50] of about 0.048%. Previous studies carried out on synthesized Fe_3O_4 obtained by co-precipitation method reported similar crystallite sizes [42]. Such outcomes suggest that the iron nanoparticle crystallite sizes are influenced by the addition of GO sheets on the surface of which they adhere.

As shown in Fig. 7, the morphology of GO, GO@Fe_3O_4 and GO@Fe_3O_4/MPc hybrid materials was studied by SEM and TEM. According to the image of Fig. 7a, it is possible to observe the stacking of the graphene oxide sheets in a multilayer arrangement, whose morphology is compatible with the profile observed in the literature [51]. At the edges of the leaves, the areas are slightly brighter, indicating that such regions are even thinner, some of which appear as formed by single layers of GO (see Fig. 7b). Figure 7c, d exhibits SEM and TEM pictures of Fe_3O_4-decorated GO sheets. Such heterostructured morphology results more clear in the TEM picture (see Fig. 7d). Fe_3O_4 nanoparticles are evenly and densely deposited reasonably on both sides of sheets according to a sandwich-like heterostructured architecture. After the functionalization either with CuPc

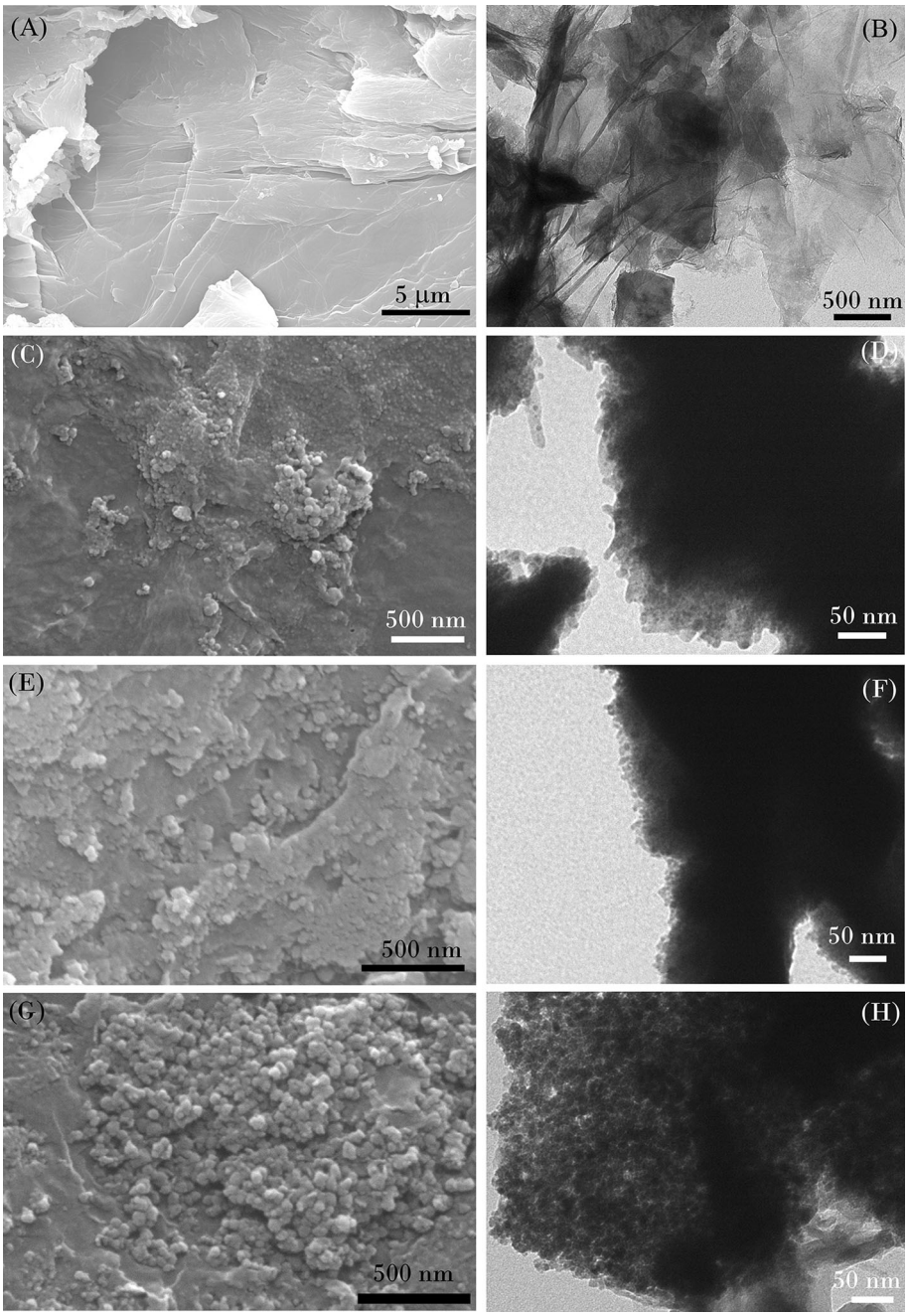

Figure 7 Micrographs of samples: GO (**a**, **b**); GO@Fe_3O_4 (**c**, **d**); GO@Fe_3O_4/CuPc (**e**, **f**) and GO@Fe_3O_4/ZnPc (**g**, **h**). The *left side* of the figure reports pictures obtained from SEM analysis, whereas images on the *right side* account for TEM investigation.

Fig. 7e, f or with ZnPc Fig. 7g, h, the shape of the heterostructures does not result significantly influenced or the density of the iron-based nanoparticles appreciable. In all probability, it can be assumed that, in the above-described nanosystems, GO acts as material–host favoring the anchoring of phthalocyanine molecules. So, according to the SEM and TEM analyses, the nanostructures can be hypothesized as formed by the adsorption of metallo-phthalocyanine into/onto the layers of graphene oxide, also containing iron nanoparticles, the latter interacting with the sheets through the π-stacking. Following the studies carried out by Yang et al. [26], the mechanism of electronic interaction between the two components is of the type π–π; namely, the sp^2 carbons contained in the domain of the GO interact with the Pc ring through the π-stacking mechanism. Moreover, the oxygen-based functional groups, especially the GO carbonyl, interact with the metallic ion of the MPcs, acting as a ligand that coordinates on the central

metal ions by a much more complex mechanism [26]. This mechanism is consistent with the bands' displacement observed in UV–Vis. All the results demonstrate the effectiveness of the solvothermal synthesis of GO@Fe_3O_4/MPc nanohybrid materials, and the sphere size of hybrid materials can be easily controlled by the addition the of phthalocyanine.

The dielectric properties of GO, GO@Fe_3O_4 and MPc-functionalized GO@Fe_3O_4 nanohybrids were measured as a function of frequency, at room temperature, with the aim at studying the effects of magnetite nanoparticles and of phthalocyanine molecules. As shown in Fig. 8a, GO@Fe_3O_4 displayed a higher dielectric constant compared with those of the other nanosized actors (GO, GO@Fe_3O_4/CuPc and GO@Fe_3O_4/ZnPc) and these values normally occurred at large frequencies. After being grafted in the GO with Fe_3O_4, there was a considerable increase in both the dielectric constant and dielectric loss. For example, the dielectric constant for GO@Fe_3O_4 at 1 kHz to 100 MHz is 3962 and 148, with an increase of 37 and 82% than that of the pure GO (2888 and 81), respectively. The substantial improvement of the dielectric properties of the nanohybrids is interpreted in light of the interfacial polarization, also known as Maxwell–Wagner–Sillars (MWS) polarization,

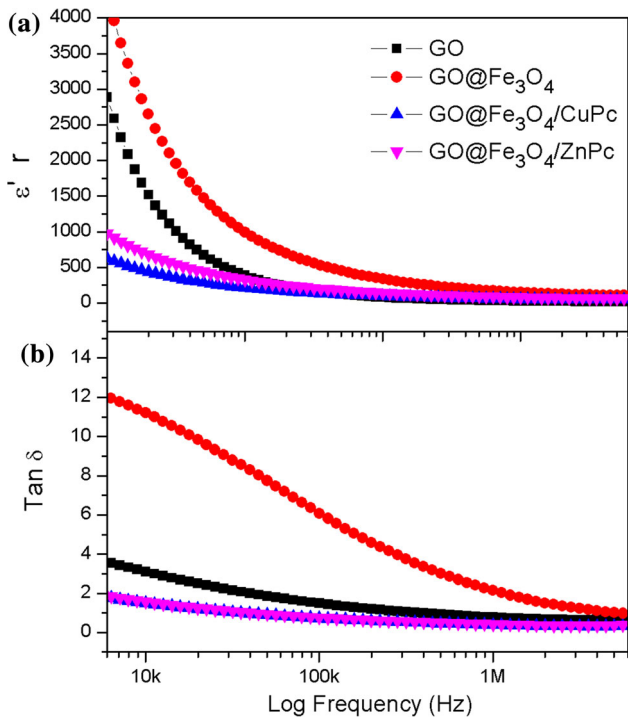

Figure 8 Behavior of **a** constant (ε'$_r$) and **b** loss (tan δ) dielectric samples.

between GO and Fe_3O_4 [52]. It is also observed that the values of ε'_r tend to decrease as a function of the amount of phthalocyanines.

A similar trend of dielectric loss (tan δ) and ε'_r, i.e., the highest and lowest values, is observed for GO@Fe_3O_4 and GO@Fe_3O_4/CuPc, respectively. The lowest values for nanohybrid are due to the interaction between the GO@Fe_3O_4 and the phthalocyanines. Thus, the combination of high aspect ratios and large surface area graphene oxide with the grafting of magnetite and phthalocyanines makes it possible to form microcapacitors. This behavior is also expected because of the CuPc and ZnPc which exhibit small values (smaller than 5 units for ε' r and less than 0.04 units for tan δ) in the microwave range, as demonstrated by Wang [53]. Another works with material based on graphene/phthalocyanines corroborated with the results obtained in the work, in which can be observed a small decrease in the values of dielectric properties after the addition of phthalocyanines [44, 54].

The lowest values of dielectric properties presented by GO@Fe_3O_4/CuPc and GO@Fe_3O_4/ZnPc make such nanomaterials good candidates as substrates for microstrip antennas, commonly referred to as the patch antennas. They are low cost, have a low profile and are easily fabricated. Thus, nanohybrid materials herein described may be thought as versatile magnetic–dielectric prototypes to be evaluated in devices operating in the microwave regime.

Conclusions

In summary, GO@ Fe_3O_4/CuPc and GO@ Fe_3O_4/ZnPc nanohybrid materials were successfully produced through a simple and effective ultrasonication method. XRD analysis showed that Fe_3O_4 nanoparticles had spinel phase with crystallize size about 12 nm and adhered to the surfaces of GO sheets. FTIR, thermal analysis, SEM and TEM confirmed the selective interaction of both Fe_3O_4 and MPcs with graphene oxide sheets. The profile of the magnetization curve of Fe_3O_4 and nanohybrids showed hysteresis, where the Ms followed a slight decrement with the incorporation of the phthalocyanines. In the nanohybrids, dielectric measurements showed the highest dielectric constant and lower losses related to the frequency between 0.1 and 6.0 MHz. These results showed that nanohybrids are materials with

superparamagnetic properties which are likely to be employed for dielectric–magnetic features. We also intend to investigate in the future applications of this material as organic dielectric materials.

Acknowledgements

This work was supported by FUNCAP, CAPES and CNPq (Brazilian agencies).

References

[1] Xu Z, Hou Y, Sun S (2007) Magnetic core/shell Fe_3O_4/Au and Fe3O4/Au/Ag nanoparticles with tunable plasmonic properties. J Am Chem Soc 129:8698–8699

[2] Selvan ST, Tan TTY, Yi DK, Jana NR (2010) Functional and multifunctional nanoparticles for bioimaging and biosensing. Langmuir 26:11631–11641

[3] Oh JK, Park JM (2011) Iron oxide-based superparamagnetic polymeric nanomaterials: design, preparation, and biomedical application. Prog Polym Sci 36:168–189

[4] Deriu MA, Popescu LM, Ottaviani MF, Danani A, Piticescu RM (2016) Iron oxide/PAMAM nanostructured hybrids: combined computational and experimental studies. J Mater Sci 51:1996–2007

[5] Sarvari MH, Khanivar A, Moeini F (2015) Magnetically recoverable nanoPd/Fe_3O_4/ZnO catalyst: preparation, characterization, and application for the synthesis of 2-oxazolines and benzoxazoles. J Mater Sci 50:3065–3074

[6] Mashhadizadeh MH, Talemi RP (2016) Synergistic effect of magnetite and gold nanoparticles onto the response of a label-free impedimetric hepatitis B virus DNA biosensor. Mater Sci Eng 59:773–781

[7] Salihov SV, Ivanenkov YA, Krechetov SP, Veselov MS, Sviridenkova NV, Savchenko AG, Klyachko NL, Golovin YI, Chufarova NV, Beloglazkina EK, Majouga AG (2015) Recent advances in the synthesis of Fe_3O_4@AU core/shell nanoparticles. J Magn Magn Mater 394:173–178

[8] Yazdani F, Fattahi B, Azizi N (2016) Synthesis of functionalized magnetite nanoparticles to use as liver targeting MRI contrast agent. J Magn Magn Mater 406:207–211

[9] Mousa NM, Khairy M, Shehab MJ (2016) Nanostructured ferrite/graphene/polyaniline using for supercapacitor to enhance the capacitive behavior. Solid State Electrochem. doi:10.1007/s10008-016-3446-6

[10] Barreto ACH, Maia FJN, Santiago VR, Ribeiro VGP, Denardin JC, Mele G, Carbone L, Lomonaco D, Mazzetto SM, Fechine PBA (2012) Novel ferrofluids coated with a renewable material obtained from cashew nut shell liquid. Microfluid Nanofluid 12:677–686

[11] Hu F, Wei L, Zhou Z, Ran Y, Li Z, Gao M (2006) Preparation of biocompatible magnetite nanocrystals for in vivo magnetic resonance detection of cancer. Adv Mater 18:2553–2556

[12] Antunes E, Rapulenyane N, Ledwaba M, Litwinski C, Chidawanyika W, Nyokong T (2013) The synthesis and characterisation of magnetic nanoparticles and their interaction with a zinc phthalocyanine. Inorg Chem Commun 29:60–64

[13] Souza NDG, Freire RM, Cunha AP, da Silva MAS, Mazzetto SE, Sombra ASB, Denardin JC, Ricardo NMPS, Fechine PBA (2015) New magnetic nanobiocomposite based in galactomannan/glycerol and superparamagnetic nanoparticles. Mater Chem Phys 156:113–120

[14] Singh K, Ohlan A, Pham VH, Balasubramaniyan RB, Varshney S, Jang J, Hur SH, Choi WM, Kumar M, Dhawan SK, Kong B-S, Chung JS (2013) Nanostructured graphene/Fe_3O_4 incorporated polyaniline as a high performance shield against electromagnetic pollution. Nanoscale 5:2411–2420

[15] Liu P, Huang Y (2013) Synthesis of reduced graphene oxide-conducting polymers-Co_3O_4 composites and their excellent microwave absorption properties. RSC Adv 41:19033–19039

[16] Yang Z, Huang R, Qi W, Tong L, Su R, He Z (2015) Hydrolysis of cellulose by sulfonated magnetic reduced graphene oxide. Chem Eng J 280:90–98

[17] Al-Ghamdi AA, Al-Turki Y, Yakuphanoglu F, El-Tantawy F (2016) Electromagnetic shielding properties of graphene/acrylonitrile butadiene rubber nanocomposites for portable and flexible electronic devices. Compos B Eng 88:212–219

[18] Zhang H, Jia S, Lv M, Shi J, Zuo X, Su S, Wang L, Huang W, Fan C, Huang Q (2014) Size-dependent programming of the dynamic range of graphene oxide—DNA interaction-based ion sensors. Anal Chem 86:4047–4051

[19] Liu H, Deng L, Zhang Z, Guan J, Yan Y, Zhu Z (2015) One-step in situ hydrothermal synthesis of SnS_2/reduced graphene oxide nanocomposites with high performance in visible light-driven photocatalytic reduction of aqueous Cr(VI). J Mater Sci 50:3207–3211

[20] Yang Y, Asiri AM, Tang Z, Du D, Lin Y (2013) Graphene based materials for biomedical applications. Mater Toda 16:365–373

[21] Dinari M, Momeni MM, Goudarzirad M (2016) Dye-sensitized solar cells based on nanocomposite of polyaniline/graphene quantum dots. J Mater Sci 51:2964–2971

[22] Liu J, Cui L, Losic D (2013) Graphene and graphene oxide as new nanocarriers for drug delivery applications. Acta Biomater 9:9243–9257

[23] Hu H, Lian H, Zu L, Jiang Y, Hu Z, Li Y, Shen S, Cui X, Liu Y (2016) Durable electromechanical actuator based on graphene oxide with in situ reduced graphene oxide electrodes. J Mater Sci 51:1376–1381

[24] Wu Q, Chen M, Chen K, Wang S, Wang C, Diao G (2016) Fe_3O_4-based core/shell nanocomposites for high-performance electrochemical supercapacitors. J Mater Sci 51: 1572–1580

[25] Wang Y, Yang C, Cheng Y, Zhang Y (2015) A molecular dynamics study on thermal and mechanical properties of graphene-paraffin nanocomposites. RSC Adv 101:82638–82644

[26] Yang J-H, Gao Y, Zhang W, Tang P, Tan J, Lu A-H, Ma D (2013) Cobalt phthalocyanine—graphene oxide nanocomposite: complicated mutual electronic interaction. J Phys Chem C 117:3785–3788

[27] Gupta RK, Tuncer H, Al-Ghamdi AA, Yol S, Dere A, Yakuphanoglu F, Farooq WA (2015) Novel optical sensor based on zinc phthalocyanine. J Nanoelectron Optoelectron 9:709–713

[28] Wan Y, Cong T, Liang Q, Li Z, Xu S, Peng Y, Luc D (2016) Facile in situ solvothermal method to synthesize ZnPc-MWCNTs composites with enhanced visible light photocatalytic activity. Ceram Int 42:2425–2430

[29] Zhong J-P, Fan Y-J, Wang H, Wang R-X, Fan L-L, Shen X-C, Shi Z-J (2013) Copper phthalocyanine functionalization of graphene nanosheets as support for platinum nanoparticles and their enhanced performance toward methanol oxidation. J Power Sources 242:208–215

[30] Oni J, Ozoemena KI (2012) Phthalocyanines in batteries and supercapacitors. Year J Porphyr Phthalocyanines 16:754–760

[31] Alamin AHE, Altindal A, Altun S, Odabaş Z (2016) Highly efficient dye-sensitized solar cells based on metal-free and copper(II) phthalocyanine bearing 2-phenylphenoxy moiety. Dyes Pigm 124:180–187

[32] Choi SA, Kim K, Lee SJ, Lee H, Babajanyan A, Friedman B, Lee K (2016) Effects of thermal preparation on Copper Phthalocyanine organic light emitting diodes. J Lumin 171:149–153

[33] Linares-Flores C, Mendizabal F, Arratia-Pérez R, Inostroza N, Orellana C (2015) Substituents role in zinc phthalocyanine derivatives used as dye-sensitized solar cells. A theoretical study using density functional theory. Chem Phys Lett 639:172–177

[34] Zhen L, Guan W, Shang L, Liu M, Liu G (2008) Organic thin-film transistor memory with gold nanocrystals embedded in polyimide gate dielectric. J Phys D 41:135111

[35] Cakir D, Goksel M, Cakir V, Durmus M, Biyiklioglu Z, Kantekin H (2015) Amphiphilic zinc phthalocyanine photosensitizers: synthesis, photophysicochemical properties and in vitro studies for photodynamic therapy. Dalton Trans 44:9646–9658

[36] Bechtold IH, Eccher J, Faria GC, Gallardo H, Molin F, Gobo NRS, De Oliveira KT, Von Seggern H (2012) New columnar Zn-phthalocyanine designed for electronic applications. J Phys Chem B 116:13554–13560

[37] Zawadzka A, Plociennik P, Strzelecki J, Korcala A, Arof AK, Sahraoui B (2014) Impact of annealing process on stacking orientations and second order nonlinear optical properties of metallophthalocyanine thin films and nanostructures. Dyes Pigm 101:212–220

[38] Yang J, Yan D, Jones TS (2015) Molecular template growth and its applications in organic electronics and optoelectronics. Chem Rev 115:5570–5603

[39] Chandra V, Park J, Chun Y, Lee JW, Hwang I, Kim KS (2010) Water-dispersible magnetite-reduced graphene oxide composites for arsenic removal. ACS Nano 4:3979–3986

[40] Hummers WS, Offeman RE (1958) Preparation of graphitic oxide. J Am Chem Soc 80:1339

[41] Attanasi OA, Ciccarella G, Filippone P, Mele G, Spadavecchia J, Vasapollo G (2003) Novel phthalocyanines containing cardanol derivatives. J Porphyr Phthalocyanines 7:52–157

[42] Barreto ACH, Santiago VR, Freire RM, Mazzetto SE, Sasaki JM, Vasconcelos IF, Denardin JC, Mele G, Carbone L, Fechine PBA (2013) Grain size control of the magnetic nanoparticles by solid state route modification. JMEPEG 22:2073–2079

[43] Giri J, Pradhan P, Somani V, Chelawat H, Chhatre S, Banerjee R, Bahadur D (2008) Synthesis and characterizations of water-based ferrofluids of substituted ferrites [$Fe_1 - xB_x Fe_2O_4$, B = Mn, Co ($x = 0$–1)] for biomedical applications. J Magn Magn Mater 5:724–730

[44] Karousis N, Sandanayaka ASD, Hasobe T, Economopoulos SP, Sarantopoulou E, Tagmatarchis N (2011) Graphene oxide with covalently linked porphyrin antennae: synthesis, characterization and photophysical properties. J Mater Chem 21:109–117

[45] Pham VH, Pham HD, Dang TT, Hur SH, Kim EJ, Kong B-S, Kim S, Chung JS (2012) Chemical reduction of an aqueous suspension of graphene oxide by nascent hydrogen. J Mater Chem 22:10530–10536

[46] Liu Y, Zhou J, Zhang X, Liu Z, Wan X, Tian J, Wang T, Chen Y (2009) Synthesis, characterization and optical limiting property of covalently oligothiophene-functionalized graphene material. Carbon 47:3113–3121

[47] Glover AJ, Cai M, Overdeep KR, Kranbuehl DE, Schniepp HC (2011) In situ reduction of graphene oxide in polymers. Macromolecules 44:9821–9829

[48] Słota R, Dyrda G, Hofer M, Mele G, Bloise E, Sole RD (2012) Novel lipophilic lanthanide bis-phthalocyanines functionalized by pentadecylphenoxy groups: synthesis, characterization and UV-photostability. Molecules 17:10738–10753

[49] Shihao Xu, Zhao Yingguo, Zheng Fangcai, Zhang Yuanguang (2016) Hollow Fe3O4@mesoporous carbon core–shell microspheres for efficient sorption of radionuclides. J Mater Sci 51:2550–2557

[50] Maia AOG, Meneses CT, Menezes AS, Flores WH, Melo DMA, Sasaki JM (2006) Synthesis and X-ray structural characterization of NiO nanoparticles obtained by gelatin. J Non-Cryst Solids 352:3729–3733

[51] Bayer T, Cunning BV, Selyanchyn R, Daio T, Nishihara M, Fujikawa S, Lyth SM (2016) Alkaline anion exchange membranes based on KOH-treated multilayer graphene oxide. J Membr Sci 508:51–61

[52] Tsangaris GM, Psarras GC, Kouloumbi N (1998) Electric modulus and interfacial polarization in composite polymeric systems. J Mater Sci 33:2027–2037. doi:10.1023/A:1004398514901

[53] Wei ZWR, Liu X (2016) Preparation and dielectric properties of copper phthalocyanine/graphene oxide nanohybrids via in situ polymerization. J Mater Sci 51:4682–4690

[54] Li J, Wei J, Pu Z, Xu M, Jia K, Liu X (2016) Influence of Fe3O4/Fe-phthalocyanine decorated graphene oxide on the microwave absorbing performance. J Magn Magn Mater 399:81–87